

Chapter 3

Intensity-related Dynamics of a Ti:sapphire Laser

The stabilization of the carrier-envelope offset frequency, f_{ceo} , of a mode-locked Ti:sapphire laser is a crucial step for using its frequency comb to distribute the stability of an optical frequency standard across the optical spectrum and to microwave frequencies for remotely transferring a frequency reference. Since f_{ceo} is controlled and stabilized using the intensity of the laser, as described in Section 2.2, it is important to understand how the intensity of the Ti:sapphire laser couples to its two degrees of freedom, f_{rep} and f_{ceo} . Understanding this coupling helps to identify a regime of operation where the free-running instability of f_{ceo} is minimized and enables optimization of the scheme for stabilizing f_{ceo} .

Previously, the effect of the laser intensity on f_{ceo} has been explained in terms of the dispersion of the nonlinear index of refraction of the Ti:sapphire crystal (also referred to as self-steepening) and beam pointing variations within the laser cavity caused by nonlinear refraction at the Ti:sapphire crystal surface [30]. However, we have observed that the dependence of f_{rep} and f_{ceo} on intensity is not monotonic. Instead, f_{rep} and f_{ceo} reach extrema as the intensity is increased and for higher intensities their dependence on the laser intensity experiences a sign reversal. This turning point cannot be explained by these previous coupling models, nor is the explanation in terms of nonlinear beam steering applicable for the particular Ti:sapphire laser we are using. In this chapter I will discuss the results of detailed experimental investigations of the intensity-related

dynamics of both f_{rep} and f_{ceo} , in which we have found that the dominant mechanism for coupling the laser intensity to these parameters is an intensity-related spectral shift, as previously suggested by Xu et al [83]. The turning point in the dependence of f_{rep} and f_{ceo} on the laser intensity corresponds to an intensity-related turning point for the center of the laser spectrum. Our experimental findings are consistent with theoretical calculations predicting the intensity-related effects on the laser parameters [35, 36].

3.1 Theory of intensity-dependent mode-locking dynamics

Calculating how the intensity of the laser affects its parameters, f_{rep} and f_{ceo} , can be accomplished by first expressing f_{rep} and f_{ceo} in terms of the average group (v_g) and phase (v_p) velocities in the laser cavity. From Eqns. (2.3) and (2.6), we have

$$\begin{aligned} f_{ceo} &= f_{rep} \frac{\omega_c l_c}{2\pi} \left(\frac{1}{v_g} - \frac{1}{v_p} \right) \\ &= \frac{\omega_c}{2\pi} \left(1 - \frac{v_g}{v_p} \right) \end{aligned} \quad (3.1)$$

since f_{rep} is given by

$$f_{rep} = \frac{v_g}{l_c} \quad (3.2)$$

where ω_c is the spectrally weighted center frequency and l_c is the round-trip cavity length. For this analysis the laser cavity is approximated as a homogeneous medium, with an average index of refraction \bar{n} defined such that the product $\bar{n}l_c$ is equivalent to the true optical path length through the air and Ti:sapphire crystal during a cavity round trip. \bar{n} contains the nonlinear contribution to the index of refraction as well, and can be written as $\bar{n} = \bar{n}_0 + \bar{n}_2 \hat{I}$ where \bar{n}_0 and \bar{n}_2 are also average values for the laser cavity and \hat{I} represents the pulse peak intensity of the laser within the Ti:sapphire crystal. Both v_p and v_g can be expressed in terms of \bar{n} . v_p is expressed simply as

$$v_p = \frac{c}{\bar{n}} = \frac{c}{\bar{n}_0 + \bar{n}_2 \hat{I}} \quad (3.3)$$

However, because of the nonlinearity, the expression for v_g is not simply $(dk/d\omega)^{-1}$, but instead is given by

$$v_g = \frac{c}{\bar{n}_0 + \omega_c \left(\frac{d\bar{n}_0}{d\omega} \right)_{\omega_c} + 3 \left[\bar{n}_2 + \omega_c \left(\frac{d\bar{n}_2}{d\omega} \right)_{\omega_c} \right] \hat{I}} \quad (3.4)$$

Appendix A provides a derivation of this expression. Note that naively using $(dk/d\omega)^{-1}$ would result in a very similar expression, with the coefficient of the nonlinear contribution changed from a 3 to a 1.

The dependence of the frequencies f_{rep} and f_{ceo} on the pulse peak intensity in the crystal, \hat{I} , is found by differentiating Eqns. (3.1) and (3.2) with respect to \hat{I} , yielding

$$\frac{df_{rep}}{d\hat{I}} = \frac{1}{l_c} \frac{dv_g}{d\hat{I}} \quad (3.5)$$

$$\frac{df_{ceo}}{d\hat{I}} = \frac{1}{2\pi} \frac{\partial\omega_c}{\partial\hat{I}} \left(1 - \frac{v_g}{v_p} \right) + \frac{\omega_c v_g}{2\pi v_p} \left(\frac{1}{v_p} \frac{dv_p}{d\hat{I}} - \frac{1}{v_g} \frac{dv_g}{d\hat{I}} \right) \quad (3.6)$$

The term $\partial\omega_c/\partial\hat{I}$ is the intensity-related laser spectral shift. From Eqn. (3.4) it is clear that the dependence of v_g on \hat{I} enters explicitly, as well as through its dependence on ω_c . Therefore

$$\frac{d}{d\hat{I}} \left(\frac{1}{v_g} \right) = \frac{\partial\omega_c}{\partial\hat{I}} \frac{\partial}{\partial\omega_c} \left(\frac{1}{v_g} \right) + \frac{3}{c} \left[\bar{n}_2 + \omega_c \left(\frac{d\bar{n}_2}{d\omega} \right)_{\omega_c} \right] \quad (3.7)$$

From Eqn. (3.3) we see that v_p also depends on \hat{I} explicitly and through ω_c (\bar{n} depends on ω_c through dispersion), and so

$$\frac{d}{d\hat{I}} \left(\frac{1}{v_p} \right) = \frac{1}{c} \left(\frac{\partial\omega_c}{\partial\hat{I}} \frac{\partial\bar{n}}{\partial\omega_c} + \bar{n}_2 \right) \quad (3.8)$$

Rewriting Eqn. (3.5) and plugging in (3.7) gives the dependence of f_{rep} on \hat{I} .

$$\begin{aligned} \frac{df_{rep}}{d\hat{I}} &= -\frac{v_g^2}{l_c} \frac{d}{d\hat{I}} \left(\frac{1}{v_g} \right) \\ &= -\frac{1}{l_c} \frac{v_g^2}{c} \left[\frac{\partial\omega_c}{\partial\hat{I}} \frac{\partial}{\partial\omega_c} \left(\frac{1}{v_g} \right) + 3\bar{n}_2 + 3\omega_c \left(\frac{d\bar{n}_2}{d\omega} \right)_{\omega_c} \right] \end{aligned} \quad (3.9)$$

The same can be done for f_{ceo} using Eqns. (3.6), (3.7), and (3.8).

$$\begin{aligned}
\frac{df_{ceo}}{d\hat{I}} &= \frac{1}{2\pi} \frac{\partial\omega_c}{\partial\hat{I}} \left(1 - \frac{v_g}{v_p}\right) + \frac{\omega_c v_g}{2\pi v_p} \left[-v_p \frac{d}{d\hat{I}} \left(\frac{1}{v_p}\right) + v_g \frac{d}{d\hat{I}} \left(\frac{1}{v_g}\right)\right] \\
&= \frac{1}{2\pi} \frac{\partial\omega_c}{\partial\hat{I}} \left[1 - \frac{v_g}{v_p} - \frac{\omega_c v_g}{c} \frac{\partial\bar{n}}{\partial\omega_c} + \frac{\omega_c v_g^2}{v_p} \frac{\partial}{\partial\omega_c} \left(\frac{1}{v_g}\right)\right] \\
&\quad + \frac{\omega_c v_g}{2\pi c v_p} \left[3\bar{n}_2 v_g - \bar{n}_2 v_p + 3v_g \omega_c \left(\frac{d\bar{n}_2}{d\omega}\right)_{\omega_c}\right] \tag{3.10}
\end{aligned}$$

All of the terms in Eqns. (3.9) and (3.10) are constants taken from the literature, except $\partial\omega_c/\partial\hat{I}$ and $\partial(v_g^{-1})/\partial\omega_c$. The first term in (3.9) and the first set of brackets in (3.10) reveal the dependence on the intensity-related spectral shift. Both equations are dominated by the term proportional to $(\partial\omega_c/\partial\hat{I})(\partial(v_g^{-1})/\partial\omega_c)$, explaining the near coincidence in the sign change of $df_{rep}/d\hat{I}$ and $df_{ceo}/d\hat{I}$ with that of $\partial\omega_c/\partial\hat{I}$. This also reveals that the spectral shift couples to the laser parameters through the group-delay dispersion (GDD) of the laser cavity, which is proportional to $\partial(v_g^{-1})/\partial\omega_c$. From the dependence of f_{rep} on the pulse peak intensity, given in Eqn. (3.9), an experimental measurement of $df_{rep}/d\hat{I}$ and $\partial\omega_c/\partial\hat{I}$ will uniquely determine the dependence of the average group velocity on the laser spectrum, $\partial(v_g^{-1})/\partial\omega_c$. This value can then be used in conjunction with $\partial\omega_c/\partial\hat{I}$ to calculate the dependence of f_{ceo} on the peak intensity, using Eqn. (3.10), which can be compared with an experimental measurement of $df_{ceo}/d\hat{I}$.

An evaluation of these expressions requires several parameters of the laser. The Ti:sapphire laser we are using has a repetition frequency of 750 MHz, corresponding to a round-trip cavity length of $l_c = 0.4$ m, and has a ring configuration. The generation of short pulses from a mode-locked Ti:sapphire laser requires that the GDD of the crystal and other intracavity elements be compensated, such that during operation the net intracavity GDD is zero. This laser utilizes specially designed mirrors for the dispersion compensation, so the only intracavity transmission element is the crystal. Therefore, the average linear contribution to the refractive index is calculated from $\bar{n}_0 l_c = (l_c - l_{Ti}) + n_0^{Ti} l_{Ti}$. Using 2.4 mm for the length of the crystal, l_{Ti} , and 1.76 for the index of refraction of the crystal, n_0^{Ti} , yields $\bar{n}_0 = 1.00456$. Its disper-

sion is found using $d\bar{n}_0/d\omega = (l_{Ti}/l_c)(dn_0^{Ti}/d\omega)$, which gives $d\bar{n}_0/d\omega = 6 \times 10^{-20}$ s. The contribution from the mirrors to $d\bar{n}_0/d\omega$ is approximated by attributing the pulse delay to a reasonable dielectric thickness and is found to be negligible. The average nonlinear contribution to the refractive index is computed by taking into account Gaussian beam propagation through the crystal. With a TEM_{0,0} laser mode, $\bar{n}_2 \hat{I}_c = n_2^{Ti} \int_{-l_{Ti}/2}^{l_{Ti}/2} I(z) dz = n_2^{Ti} \hat{I} \int_{-l_{Ti}/2}^{l_{Ti}/2} [1 + (z/z_0)^2]^{-1} dz$. z_0 indicates the Rayleigh range of the mode [78] and can be computed from the beam waist inside the crystal, which is 10 μm . From this expression, it is found that $\bar{n}_2 \sim 7.3 \times 10^{-23} \text{ m}^2 \text{ W}^{-1}$. The ratio \bar{n}_2/n_2 is used to scale $dn_2/d\omega$ to find $d\bar{n}_2/d\omega$. Using the value of $dn_2/d\omega$ calculated in [30] yields $d\bar{n}_2/d\omega \sim 1.2 \times 10^{-38} \text{ s m}^2 \text{ W}^{-1}$. Finally, conversion from the experimentally measured value of the average laser output power, P , to the pulse peak intensity within the crystal, \hat{I} , is accomplished with the expression $\hat{I} = (2P)/(T\Delta\tau f_{rep}\pi w_0^2)$, where T is the output coupling and $\Delta\tau$ is the temporal width of the pulse. For a sech^2 pulse, $\Delta\tau$ is given by $\Delta\nu\Delta\tau = 0.315$, where $\Delta\nu$ is the pulse bandwidth in frequency [16]. The output coupling and pulse bandwidth are respectively 3% and ~ 22 nm, which give $\hat{I} = (10^{16} \text{ m}^{-2}) P$.

3.2 Experimental investigation of intensity-related dynamics

The intensity-related dynamics of the Ti:sapphire laser are experimentally measured using two different approaches. For the measurement of the low-bandwidth response, a direct-frequency-counting technique is used to track f_{rep} and f_{ceo} . For determining the response of f_{ceo} at Fourier frequencies higher than a few Hertz, a frequency-to-voltage (f-V) converter is used to measure its fluctuations. These two schemes are summarized in Fig. 3.1. In both scenarios, the intensity of the laser is varied by adjusting the pump power using an AOM in the pump beam. Using a modulation signal summed with an adjustable DC bias to control the power of the RF signal driving the AOM allows the intensity of the laser to be modulated about an adjustable mean value.

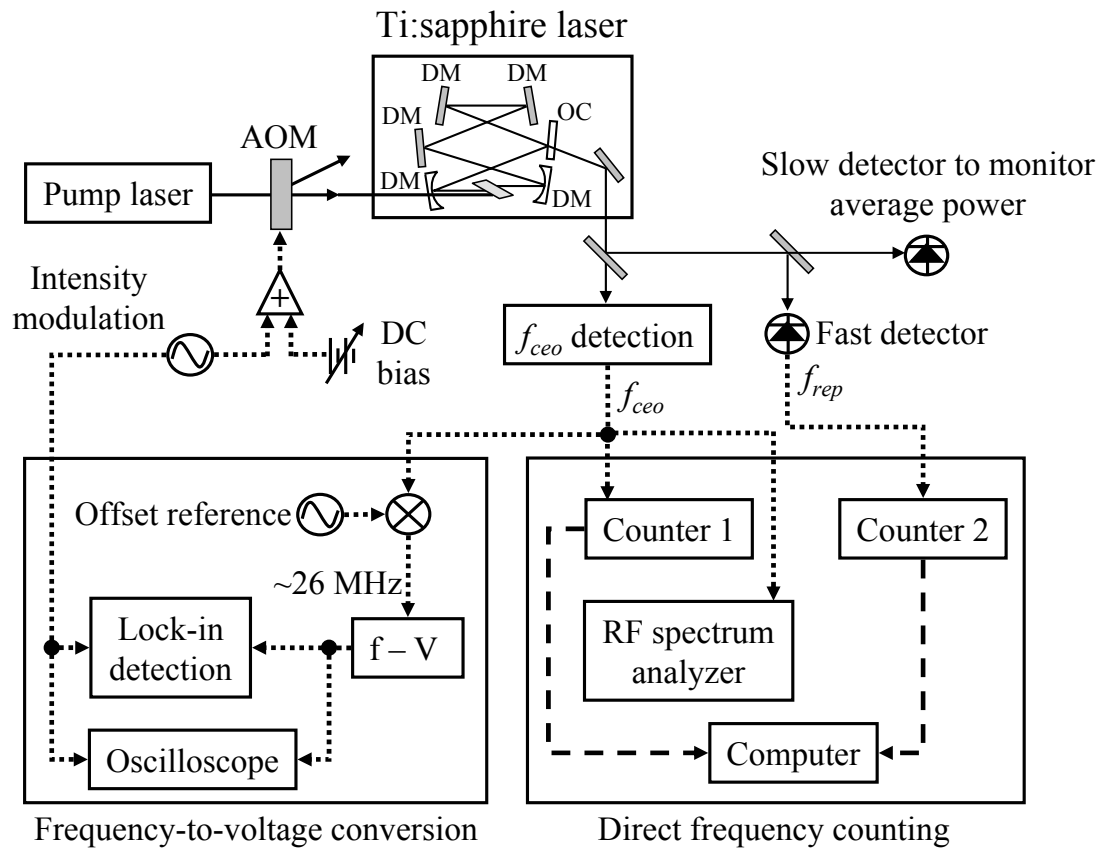


Figure 3.1: The intensity-related dynamics of the Ti:sapphire laser are measured by modulating the laser intensity and determining the response of f_{rep} and f_{ceo} . Direct frequency counting is used for low-frequency modulation and a frequency-to-voltage (f-V) converter is used to measure the fast dynamics of f_{ceo} . DM, dispersive mirrors to compensate dispersion of laser cavity; OC, output coupler of laser.

The carrier-envelope offset frequency is determined using the self-referencing technique described in Section 2.2, f_{rep} is obtained from a sufficiently fast photodetector, and the average laser output power is monitored with a low-bandwidth detector. For direct frequency counting, f_{rep} and f_{ceo} are recorded with two frequency counters operating at appropriately chosen gate times. An RF spectrum analyzer is utilized for analysis of the spectral linewidth and shape of f_{ceo} , as well as convenient readout of its mean value. The low-bandwidth response near DC is measured by sinusoidally modulating the laser intensity at ~ 0.1 Hz so that the frequency counters with a gate time of 0.1 s can track the changing frequencies with sufficient resolution and speed. Measurement of the fast dynamics of f_{ceo} using the f-V converter is accomplished by mixing the f_{ceo} signal with a stable microwave frequency reference to produce a difference-frequency that falls within the input frequency range of the f-V converter. The response of f_{ceo} is determined from the amplitude of the oscillations of the voltage output from the f-V converter. This amplitude is measured using lock-in detection for sinusoidal modulation of the laser intensity at frequencies < 100 kHz, and using an oscilloscope for frequencies > 100 kHz up to 400 kHz. The frequency response (transfer function) of the f-V converter is carefully measured so that the true response of the laser can be extracted after removing the response of the f-V converter.

Figure 3.2 illustrates the intensity dependence of the center frequency of the pulse spectrum, ω_c , and f_{ceo} . These results are obtained by adjusting the DC bias in Fig. 3.1 that controls the pump power and recording the values of ω_c , f_{ceo} , and the Ti:sapphire laser average output power at each position. The values for ω_c are determined from the weighted averages of the pulse spectrum measured with an optical spectrum analyzer. Under certain conditions, variation of the pump power may result in the emergence of cw lasing components from the Ti:sapphire laser in addition to the pulse spectrum. These cw frequency components can have a significant influence on the pulse dynamics. However, the ring configuration of the laser cavity makes it straightforward to detect

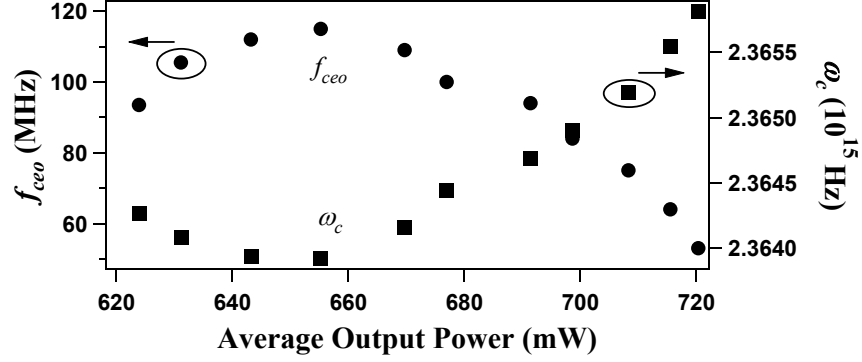


Figure 3.2: The dependence of ω_c (right axis) and f_{ceo} (left axis) on the Ti:sapphire laser average output power, which is directly related to its peak intensity, exhibits a sign reversal.

the presence of any cw components, since the pulses travel in only one direction around the cavity while the cw components will travel in both directions. Monitoring the laser output in the direction corresponding to propagation around the cavity opposite to that travelled by the pulses allows the detection of cw lasing components. The laser is adjusted to ensure that no cw components are present within the range of power variation. Also, an autocorrelation measurement confirms that the pulse width remains constant within this same range. Therefore, the measured changes in the average output power of the Ti:sapphire laser are directly related to changes in the peak intensity of the laser pulses within the laser crystal, \hat{I} , and the changes in the laser parameters can be attributed entirely to mode-locking dynamics related to the pulse peak intensity. Fig. 3.2 clearly shows that neither ω_c , shown as squares with respect to the vertical axis at right, nor f_{ceo} , displayed as circles with respect to the left vertical axis, is a monotonic function of the laser intensity. There is a change in the sign of $df_{ceo}/d\hat{I}$, which is accompanied by a sign change of $\partial\omega_c/\partial\hat{I}$. A second-order polynomial fit to the ω_c data is used to find experimental values of the intensity-related spectral shift, $\partial\omega_c/\partial\hat{I}$.

Values for $df_{rep}/d\hat{I}$ and $df_{ceo}/d\hat{I}$ near DC are determined using the direct-frequency-counting method of Fig. 3.1. Shown in Fig. 3.3 are some representative data of the slowly modulated carrier-envelope offset frequency (pluses) with fits to a sine function (solid lines) for various average values of the laser output power. Note that

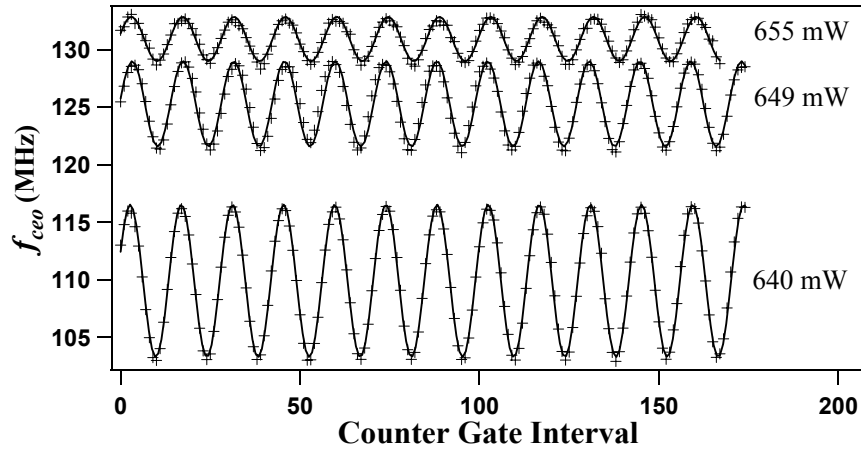


Figure 3.3: Direct frequency counting of the response of f_{ceo} to slow modulation of the laser intensity for laser powers below that corresponding to the sign change of $df_{ceo}/d\hat{I}$ (pluses), and sine function fits (solid lines). The amplitude of power modulation is nearly constant. The mean value of f_{ceo} increases with power ($df_{ceo}/d\hat{I} > 0$), whereas the response amplitude decreases as $df_{ceo}/d\hat{I}$ approaches zero.

the period of the oscillations indicated by the number of 0.1-s gate intervals per period is much shorter than that corresponding to the frequency of modulation of ~ 0.1 Hz. This is due to the significant dead time of the frequency counter between adjacent data acquisition intervals. The data in Fig. 3.3 are for laser powers below that corresponding to the sign change of $df_{ceo}/d\hat{I}$, where $df_{ceo}/d\hat{I} > 0$, and are taken using nearly the same amplitude of power modulation. Hence, as the average laser power is increased, the mean value of f_{ceo} increases, whereas its modulation response amplitude decreases as $df_{ceo}/d\hat{I}$ approaches zero. The original raw data for f_{ceo} contain a linear drift over time that is subtracted, since only the modulation amplitude is of interest. Similar data are obtained for f_{rep} . From the amplitudes of the sinusoidal fits and direct measurements of the modulation depth of the average laser output power, experimental values

of $df_{rep}/d\hat{I}$ and $df_{ceo}/d\hat{I}$ are determined. These values are shown in Fig. 3.4, with filled circles for $df_{rep}/d\hat{I}$ and open circles for $df_{ceo}/d\hat{I}$. From the experimental values of

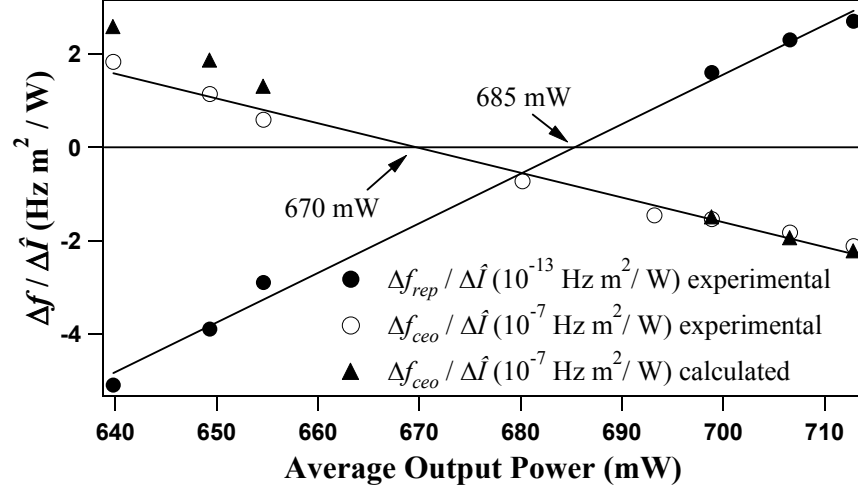


Figure 3.4: The experimental values of $\Delta f_{rep}/\Delta \hat{I}$ and $\Delta f_{ceo}/\Delta \hat{I}$ measured near DC, versus the Ti:sapphire laser average output power, confirm that there is a sign reversal of these coefficients. The values of $\Delta f_{ceo}/\Delta \hat{I}$ calculated using a parameter derived from the $\Delta f_{rep}/\Delta \hat{I}$ data are in close agreement with the experimental data.

$df_{rep}/d\hat{I}$ and $\partial\omega_c/\partial\hat{I}$, the values of $\partial(v_g^{-1})/\partial\omega_c$ can be computed using Eqn. (3.9). The values of $\partial(v_g^{-1})/\partial\omega_c$ are found to be negative, which is consistent with the fact that the net linear contribution to the GDD in the laser cavity must be negative to compensate for the effective positive nonlinear contribution during operation from the self-phase modulation in the crystal. The calculated values of $\partial(v_g^{-1})/\partial\omega_c$ are used in combination with the experimental values of $\partial\omega_c/\partial\hat{I}$ to compute $df_{ceo}/d\hat{I}$ via Eqn. (3.10), with the results shown as triangles in Fig. 3.4. These calculated values of $df_{ceo}/d\hat{I}$ are in good agreement with the directly measured data, showing that the equations for $df_{rep}/d\hat{I}$ and $df_{ceo}/d\hat{I}$, (3.9) and (3.10), are consistent with the experimental data.

The dynamic response of f_{ceo} to modulation of the Ti:sapphire laser intensity at frequencies higher than a few Hertz is determined using the f-V converter as shown in Fig. 3.1. The response of f_{ceo} and the depth of intensity modulation are measured for modulation frequencies ranging from 10 Hz to 400 kHz at three different values

of average laser power. These data of the transfer function of f_{ceo} , $\Delta f_{ceo}/\Delta \hat{I}$ versus modulation frequency, for the three values of average laser power are shown in Fig. 3.5. (The data were taken at a different time than those in the previous figures, and f_{ceo} reaches a maximum at a higher average laser power of ~ 755 mW instead of ~ 660 mW.) The two sets of data taken at average powers of 711 mW and 744 mW (squares and

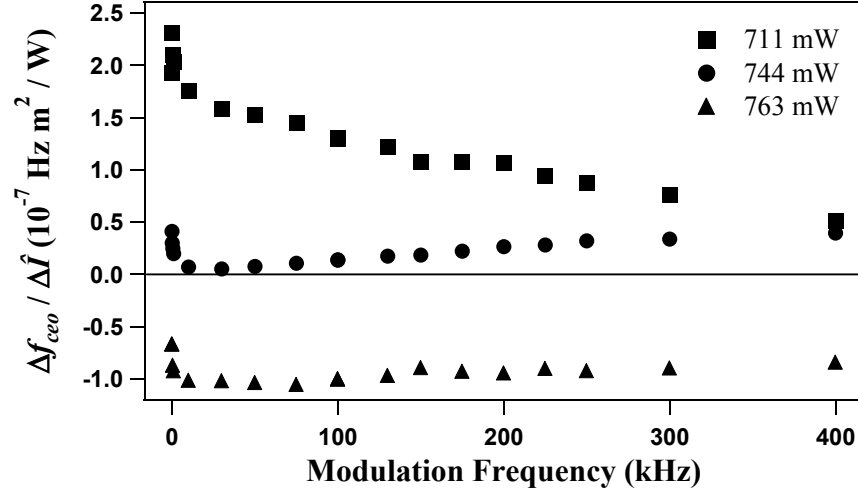


Figure 3.5: The dynamic response (transfer function) of f_{ceo} is shown for two laser powers where $df_{ceo}/d\hat{I} > 0$ and for one value of the laser power where $df_{ceo}/d\hat{I} < 0$. Notice that although the fast response changes sign accordingly, the thermal response near DC always provides a positive contribution.

circles, respectively) correspond to powers below the zero-crossing point of $df_{ceo}/d\hat{I}$ ($df_{ceo}/d\hat{I} > 0$). The third data set taken at an average power of 763 mW (triangles) corresponds to a region of operation where $df_{ceo}/d\hat{I} < 0$. The step rise in response toward DC for Fourier frequencies below 1 kHz is attributed to thermal effects in the Ti:sapphire crystal. Above 1 kHz, however, the response is roughly flat, at least over the measured frequency range extending to 400 kHz. Notice that although the fast response of f_{ceo} does change sign, following the sign of $df_{ceo}/d\hat{I}$, the sign of the thermal response is unaffected by the sign change of $df_{ceo}/d\hat{I}$. This can be seen by the fact that the response of f_{ceo} approaches zero for modulation frequencies approaching DC for the

763-mW data (where $df_{ceo}/d\hat{I} < 0$). The increased positive thermal response partially cancels the negative response related to the fast mode-locking pulse dynamics.

3.3 Investigation of lineshape of carrier-envelope offset frequency

In addition to directly measuring $df_{ceo}/d\hat{I}$, the dynamics of f_{ceo} can be studied by examining its spectral linewidth and shape. The value of f_{ceo} and its spectral linewidth are measured with an RF spectrum analyzer for several values of the average Ti:sapphire laser power, both above and below the turning point of f_{ceo} . These data, which represent a DC measurement of the intensity dependence of the mean value of f_{ceo} , are shown in the upper portion of Fig. 3.6. In the bottom panel of this figure are the experimental values of $df_{ceo}/d\hat{I}$ versus average laser power obtained for intensity modulation at 10 kHz. From the data in Fig. 3.5, it is evident that when $df_{ceo}/d\hat{I} = 0$ for modulation at 10 kHz, a DC measurement of $df_{ceo}/d\hat{I}$ will produce a positive result because of the positive thermal response at DC. Therefore, a DC measurement will find that $df_{ceo}/d\hat{I} = 0$ at a higher power, where the fast response is negative and cancels the positive thermal response. This is supported by Fig. 3.6, where the extremum of the f_{ceo} data taken at DC occurs at a higher power than that corresponding to the zero-crossing of $df_{ceo}/d\hat{I}$ obtained with 10-kHz modulation. In addition, the lineshapes in the upper portion of Fig. 3.6 reveal that the phase noise of f_{ceo} increases dramatically when $df_{ceo}/d\hat{I}$ deviates from zero, and is at a minimum when $df_{ceo}/d\hat{I} = 0$ when measured at 10-kHz modulation (not at the extremum for the DC measurements). This indicates that the dominant source of phase variations of f_{ceo} is fast fluctuations of the pulse intensity, since the linewidth of f_{ceo} is at a minimum at the position where it is decoupled from such fast fluctuations. Attributing the phase variations of f_{ceo} to intensity fluctuations can be verified by considering the rms power fluctuations of the pump laser, provided by the laser manufacturer. The given value of 0.02% for rms power fluctuations of the pump laser is converted into frequency noise using the measured

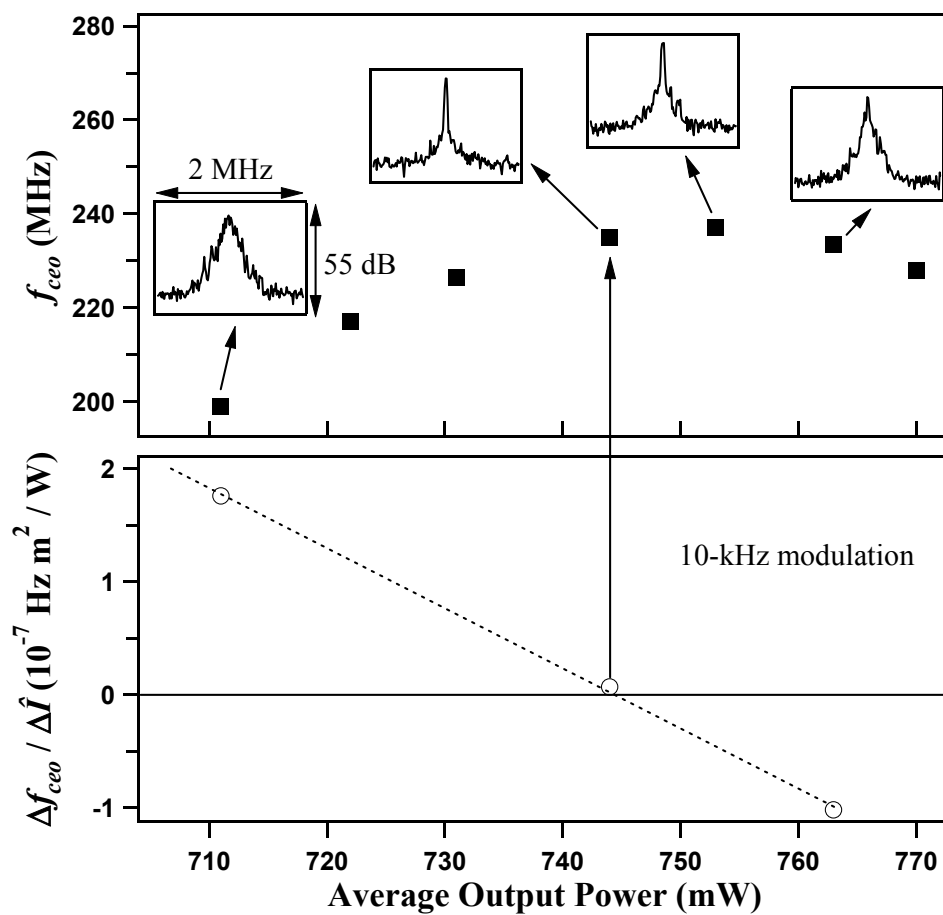


Figure 3.6: Top: The linewidth of f_{ceo} for average laser powers above and below that corresponding to $df_{ceo}/d\hat{I} = 0$, with corresponding mean values for f_{ceo} obtained at DC. The lineshape traces are obtained with a 10-kHz resolution bandwidth. Bottom: The response of f_{ceo} to intensity measured at 10-kHz modulation.

coefficients for the dependence of f_{ceo} on the Ti:sapphire laser intensity and the dependence of the laser intensity on the pump power. For the first value of f_{ceo} in Fig. 3.6, at 197 MHz, this conversion produces an rms frequency noise of ~ 200 kHz. In comparison, the measured width of the corresponding lineshape in Fig. 3.6 is ~ 500 kHz. For the next-to-last f_{ceo} data point shown in Fig. 3.6, the pump power fluctuations predict an rms frequency noise of ~ 100 kHz, half that predicted for the first value. Indeed, the measured linewidth for this point is ~ 300 kHz, roughly half that measured for the first point. The linewidths predicted solely by power fluctuations of the pump laser are in rough agreement with those measured.

The universality of our results for different Ti:sapphire laser systems can be verified by studying a system that uses a different scheme for compensating the GDD in the laser cavity, which exhibits a linewidth for f_{ceo} that is much smaller than is typically achieved for the system I have been discussing. Whereas the system discussed until now uses dispersive mirrors for dispersion compensation, an alternate method for compensating dispersion relies on a pair of prisms inside the laser cavity [22, 71]. A typical lineshape of f_{ceo} for the Ti:sapphire laser system with prisms is shown on the right in Fig. 3.7. This is as much as an order of magnitude narrower than the typical lineshape for the prismless system, which exhibits a comparable linewidth only near the turning point of f_{ceo} . For comparison, the narrowest lineshape obtained for the prismless system is also shown in Fig. 3.7. It is often the case for the prismless laser that only near the position of the narrowest lineshape close to the turning point can f_{ceo} be phase-locked to a microwave reference and achieve a linewidth equivalent to that of the reference. Shown in the inset of Fig. 3.7 is such a phase-locked narrow linewidth approaching 10 mHz, which is not resolved by the 10-Hz resolution bandwidth of the figure. On the other hand, when $df_{ceo}/d\hat{I}$ is tuned away from zero, it becomes increasingly difficult to phase-lock f_{ceo} to a microwave reference and achieve such a narrow lineshape.

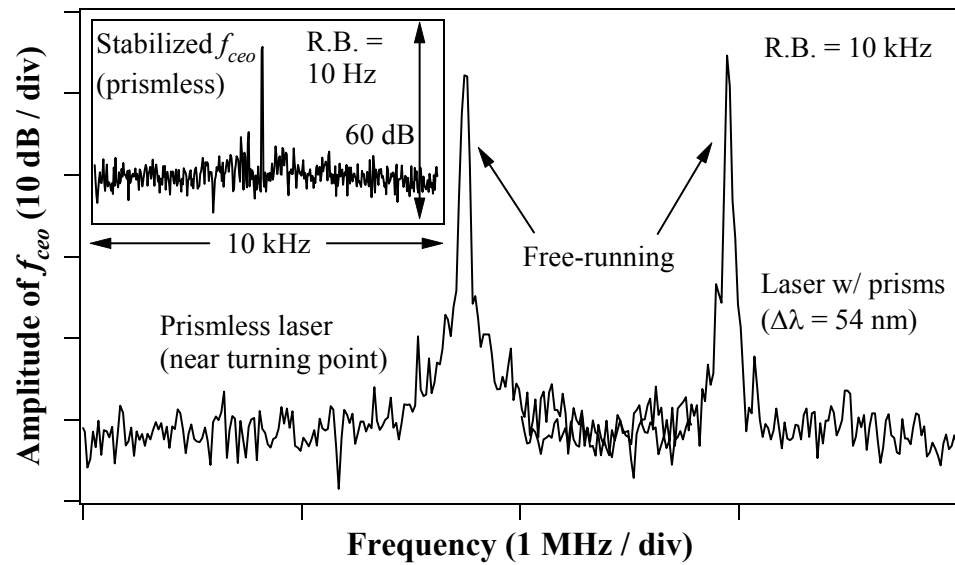


Figure 3.7: The typical lineshape of f_{ceo} for the Ti:sapphire laser incorporating prisms, recorded for a spectral bandwidth of 54 nm, is compared to the narrowest lineshape obtained for the prismless system. The inset shows the resolution-limited linewidth of f_{ceo} phase-locked to a microwave reference for the prismless system. This narrow lineshape is often only achieved when operating near the turning point. R.B., resolution bandwidth.

To understand the physical mechanisms responsible for the smaller linewidth of the system with prisms, its dynamics are studied as the insertion of one of the prisms into the cavity mode is varied. The insertion changes both the width of the pulse spectrum and the magnitude of the linear contribution to the net GDD of the laser cavity. Figure 3.8 shows the linewidths of f_{ceo} corresponding to various pulse spectral widths [full-width at half-maximum (FWHM)]. These data show that the f_{ceo} linewidth

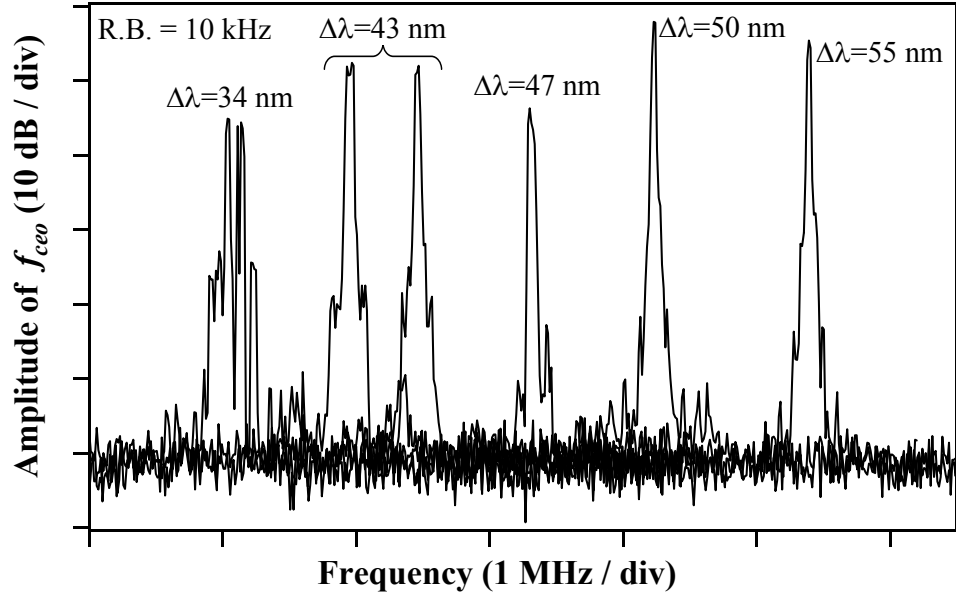


Figure 3.8: The linewidths of f_{ceo} for the Ti:sapphire laser system with prisms corresponding to various pulse spectral widths show that the linewidth decreases with increasing spectral width up to ~ 47 nm, above which the linewidth is constant. R.B., resolution bandwidth.

decreases as the width of the pulse spectrum increases, until the spectral width reaches about 47 nm. For spectra broader than ~ 47 nm, the linewidth is nearly constant. This behavior is consistent with our model attributing the noise of f_{ceo} to intensity fluctuations of the laser, which becomes apparent when the response of f_{ceo} to intensity modulation is measured for various pulse spectral widths. This data is shown in Fig. 3.9, which reveals a threshold behavior where $df_{ceo}/d\hat{I}$ decreases sharply with increasing spectral width up to a bandwidth of ~ 47 nm, above which $df_{ceo}/d\hat{I}$ remains constant

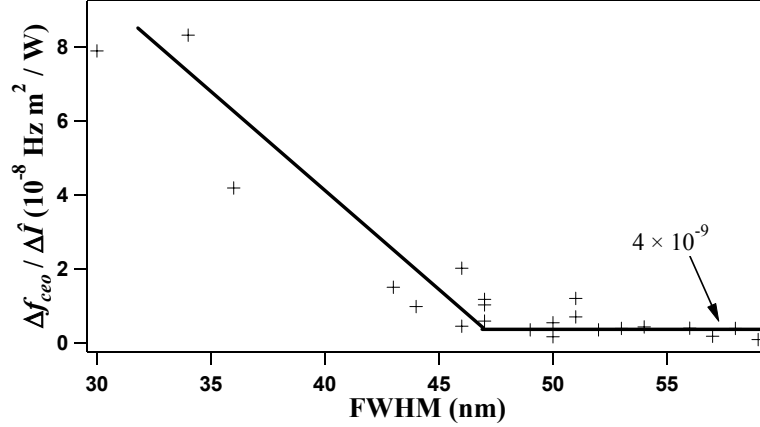


Figure 3.9: The intensity dependence of f_{ceo} for the laser system with prisms drops sharply with increasing pulse spectral width until ~ 47 nm, above which it is constant.

at $\sim 4 \times 10^{-9} \text{ Hz m}^2 \text{ W}^{-1}$. The broader spectral bandwidth and corresponding decrease in the magnitude of the linear contribution to the net cavity GDD both reduce the intensity dependence of f_{ceo} by reducing the magnitude of $\partial\omega_c/\partial\hat{I}$ and $\partial(v_g^{-1})/\partial\omega_c$, respectively. Therefore, for both the prismless system and the system with prisms, a decrease in the magnitude of the intensity-dependent spectral shift and / or the linear contribution to the net cavity GDD reduces the coupling of f_{ceo} to intensity fluctuations, thereby minimizing the free-running linewidth of f_{ceo} . The fact that for all recorded pulse bandwidths shown in Fig. 3.9, the magnitude of $df_{ceo}/d\hat{I}$ for the system with prisms is approximately ten times smaller than it is for the prismless system, as shown in Fig. 3.4, explains why in general the f_{ceo} linewidth for the prism system is smaller than that of the prismless laser.

3.4 Conclusions

The experimental results and supporting theoretical calculations demonstrate that the peak pulse intensity of the Ti:sapphire laser couples to the laser parameters, f_{rep} and f_{ceo} , through an intensity-related shift of the pulse spectrum. Changes in the pulse spectrum directly affect f_{rep} and f_{ceo} through the linear contribution to the GDD

of the laser cavity, and the turning point of the laser parameters with increasing pulse intensity is due to a corresponding turning point for the center of the spectrum. In a previous effort to explain the intensity-dependence of the parameters of the frequency comb produced by a mode-locked laser, the dependence of the group and phase velocities of solitons on the pulse energy was modeled [27]. However, although it was noted in that work that a spectral shift could cause a change in the group velocity, the model that was developed did not account for this possibility and only included effects from the Kerr nonlinearity. Our results clearly demonstrate that this model is not an accurate description of the intensity-related effects occurring in an active laser cavity and that the dominant mechanism for intensity coupling is an intensity-related spectral shift. There are two possible explanations for this intensity-induced spectral shift. The first is stimulated Raman scattering in the laser crystal, which causes a redshift of the pulse spectrum with increasing pulse energy [47, 28]. The second is a mismatch between the gain band of the laser and the loss band, determined by the mirrors, the output coupler, and reabsorption in the laser crystal. An increase in the laser intensity will reduce the gain due to multipass gain saturation, which will shift the net-gain maximum and the peak of the laser spectrum [47].

Also, our experimental investigations have identified fast fluctuations of the laser intensity as the dominant source of phase noise of f_{ceo} . For the laser system using a pair of intracavity prisms for dispersion compensation, it is possible to tune the GDD of the cavity to reduce the coupling of the intensity noise to f_{ceo} and achieve a narrow f_{ceo} lineshape. However, for the system using dispersive mirrors instead of prisms, the linear contribution to the net cavity GDD is fixed. The calculation of $\partial(v_g^{-1})/\partial\omega_c$ from our experimental data indicates this is $\sim -400 \text{ fs}^2$. Therefore, for the prismless system the intensity can only be decoupled from f_{ceo} by reducing the intensity-dependent spectral shift. This explains why the free-running lineshape of f_{ceo} for this system occurs near the position where $\partial\omega_c/\partial\hat{I} = 0$. A reduction in the spectral shift may also contribute

to the minimization of the intensity dependence of f_{ceo} for pulse bandwidths exceeding ~ 47 nm in the system using prisms, since a broad bandwidth limits the amount of spectral shift that can occur.

Our results have important implications for the stabilization of f_{ceo} using the laser intensity. At first it would seem that it is desirable to operate with the narrowest free-running f_{ceo} linewidth. However, this corresponds to operation where $df_{ceo}/d\hat{I} = 0$, which would make it impossible to stabilize f_{ceo} with the laser intensity. It is also important to not operate the laser too close to this position, since the intensity would have to be changed dramatically to affect f_{ceo} , resulting in a large amount of intensity noise on the laser. The stabilization of f_{ceo} is optimized when the laser is operated sufficiently close to the position of $df_{ceo}/d\hat{I} = 0$ to minimize the dependence of f_{ceo} on the fast intensity fluctuations outside the bandwidth of the stabilization loop, while being far enough away to use the lower-bandwidth response of f_{ceo} for stabilization. In some cases it is also possible to select the sign of the intensity dependence of f_{ceo} such that the intensity noise on the laser is suppressed when f_{ceo} is stabilized, as demonstrated in [59]. However, operating with the incorrect sign for $df_{ceo}/d\hat{I}$ could increase the intensity noise during stabilization of f_{ceo} .